ORCA – Online Research @ Cardiff

Tuning of catalytic sites in Pt/TiO₂ catalysts for the chemoselective hydrogenation of 3-nitrostyrene

Margherita Macino,[a] Alexandra J. Barnes,[a] Sultan M. Althahban,[b] Ruiyang Qu,[c,d] Emma Gibson[e], David J Morgan[a], Simon J. Freakley[a], Nikolaos Dimitratos[a,f], Christopher J. Kiely,[a,b] Xiang Gao,[c,d] Andrew M. Beale,[g,h] Donald Bethell,[i] Qian He,[a] Meenakshisundaram Sankar,[a]* and Graham J. Hutchings[a]*

[a] *Cardiff Catalysis Institute, Cardiff University, Main Building, Park Place, Cardiff CF10.3AT, UK.*

[b] *Department of Materials Science and Engineering, Lehigh University, 5 East Packer Avenue, Bethlehem, PA 18015-3195, USA.*

[c] *State Key Laboratory of Clean Energy Utilization, College of Energy Engineering, Zhejiang University, Hangzhou, 310027, China.*

[d] *Institute for Thermal Power Engineering, Zhejiang University, Hangzhou, 310027, P. R. China.*

[e] *School of Chemistry, Joseph Black Building, University Avenue, Glasgow, G12 8QQ, UK*

[f] *Department of Industrial Chemistry "Toso Montanari", Alma Mater Studiorum-University of Bologna, 40136 Bologna, Italy.*

[g] *UK Catalysis Hub, Research Complex at Harwell (RCaH), Rutherford Appleton Laboratory, Harwell Oxon, OX11 0FA, UK.*

[h] *Department of Chemistry, University College London, 20 Gordon Street, London, WC1H 0AJ, UK.*

[i] *Department of Chemistry, University of Liverpool, Liverpool L69 3BX, UK.*

Corresponding Authors: Dr. M. Sankar, Cardiff University, Email: Sankar@cardiff.ac.uk ; Prof. G. J. Hutchings, Cardiff University, Email: Hutch@cardiff.ac.uk.

Abstract

Tuning the catalytic activities of supported metal nanoparticles can be achieved by manipulating their structural properties using an appropriate design and synthesis strategy. Each step in a catalyst synthesis method can potentially play an important role in preparing the most efficient catalyst for a particular chemical reaction. Here we report the careful manipulation of the post-synthetic heat treatment procedure, together with control over the the amount of metal loading, to prepare a highly efficient 0.2 wt.% Pt/TiO_2 catalyst for the chemoselective hydrogenation of 3-nitrostyrene. We found that for Pt/TiO_2 catalysts with 0.2 and 0.5wt.% loading levels, reduction alone at 450 °C induces the coverage of Pt nanoparticles by TiO_x through a strong metal support interaction which is detrimental for their catalytic activities. However, this surface coverage can be avoided by combining a calcination treatment at 450 °C with a subsequent reduction treatment at 450 °C allowing us to prepare a exceptionally active Pt/TiO_2 catalyst with the optimum Pt distribution. Detailed characterisation of these catalysts has revealed that the peripheral sites at the Pt metal/TiO_2 support interface are the most likely active sites for this hydrogenation reaction.

Introduction

Supported metal nanocatalysts play a crucial role in our endeavour to develop new technologies for energy and environmental applications, including the production of fine chemicals and fuels from renewable and sustainable feedstock while at the same time achieving reduced emission targets.[1,2] Selective hydrogenation reactions, catalysed by supported metal nanoparticles, are one of the most widely studied reactions in academia and industry.[3] One typical example is the hydrogenation of nitroarenes to produce functionalised anilines, which are commonly used in the production of a number of fine and bulk chemicals including polymers, fertilisers, pharmaceuticals, dyes and biologically active compounds.[4,5] Recently researchers have focused on the chemoselective hydrogenation of nitro aromatics to form anilines, especially in the presence of other reducible groups such as C=C, C=O, C≡C and C≡N, because of the high synthetic value of these compounds[6,7] Many reduction processes in industry still make use of stoichiometric reducing agents like sodium hydrosulphite (or H_2S), iron in acidic media (Bechamp process), stannous chloride, samarium iodide or zinc in ammonium hydroxide.[8-10] These methods are not only unselective, but also generate huge amounts of unwanted waste. Catalytic reduction, using molecular H_2, is highly desirable because of its economics and availability; it is also environmentally benign since water is the only by-product produced.[3,7,11,12] However, achieving high chemoselectivity in this reaction without adding any homogeneous additives is still challenging. When hydrogen donors such as hydrazine,[13,14] formic acid[15] or sodium borohydride[16,17] are used, high chemoselectivities for nitro group reduction can be achieved. Recent advances in controlling the structure and properties of supported metal nanoparticles have created a renewed interest in the development of better catalysts for chemoselective

hydrogenation reactions using molecular H_2.[3] For Pt/TiO$_2$ catalysts, alloying with a second metal (*e.g.,* Au, Ni or Zn) has also been reported to increase the chemoselectivity.[11] Corma *et al.* showed that monometallic Au nanoparticles (< 5nm) supported on Fe$_2$O$_3$ could increase the selectivity (up to 99%) towards nitro group reduction during the hydrogenation of nitrostyrene.[18] Zhang *et al.* reported that atomic dispersions of Pt on FeO$_x$ were very active catalysts for the chemoselective hydrogenation of nitrostyrene[19] and furthermore they found that adding alkali metals to high loading Pt/FeO$_x$ catalysts, where nanoparticles are also present, increased the chemoselectivity dramatically.[20]
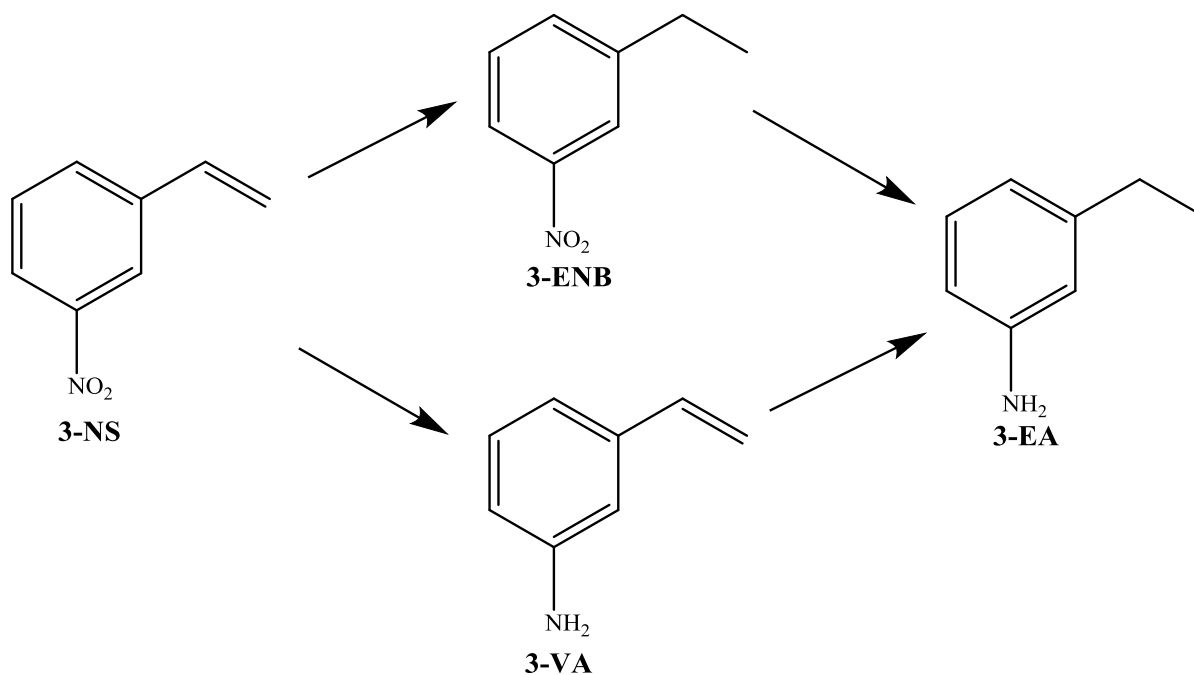
Scheme-1: *Schematic representation of the chemoselective hydrogenation of 3-nitrostyrene (3-NS) to form the desired product 3-vinylaniline (3-VA) and associated side products 3-ethylnitrobenzene (3-ENB), and 3-ethylaniline (3-EA).*

Every step in the catalyst synthesis process plays an important role in tuning the structural characteristics of the catalyst and in turn its activity, selectivity and stability. We have reported that addition of excess of chloride ions during wet-impregnation

helps in controlling the particle size and composition of supported AuPd nanoparticles.[21] Similarly, heat treatment procedures are critical in controlling metal particle size, morphology,[22] alloy formation,[21] and for removal of organic ligands or poisons, [23] thereby dramatically affecting the catalytic performance.[21,24,25] Typical heat treatments employed for hydrogenation catalysts are as follows: the as-synthesized samples are usually calcined first, to decompose the metal precursors on the support surface, followed by a gas-phase reduction, either *in-situ* or *ex-situ*, to reduce the metal ions to form the metal nanoparticles.[11,19] Corma *et al.* controlled the particle size and morphology of Pt nanoparticles supported on TiO_2, by choosing an appropriate activation temperature to tune the chemoselectivity during the hydrogenation of nitrostyrene.[11] Studies on the inter-relationship between metal loading and heat treatment are highly important, because of the current drive to reduce the metal loading to efficiently utilise scarce and expensive noble metals.[19]

Here we report the catalytic performance of 0.05 wt.%, 0.08 wt.%, 0.2 wt.% and 0.5 wt.% Pt on TiO_2 for the chemoselective hydrogenation of 3-nitrostyrene (3-NS) to 3-vinylaniline (3-VA) (Scheme-1). This substrate was selected as there are two potentially reducible groups making it a widely used model substrate for chemoselective hydrogenation reactions. The active sites have been fine-tuned by optimising the post synthesis heat treatment protocol by systematically applying different high temperature heat treatments (*i.e., either* reduction only *or* calcination only *or* calcination followed by reduction) to all these catalysts and we report the high catalytic activity displayed by the 0.2 wt.% Pt/TiO_2 *calc+red* sample. All these catalyst variants were characterised by X-ray photoelectron spectroscopy (XPS), scanning transmission electron microscopy (STEM), extended X-ray absorption fine structure (EXAFS) and X-ray absorption near edge structure (XANES) as well as CO

DRIFTS. This has allowed us to explore the complex interplay between Pt loading level, heat treatment procedure and strong metal support interactions (SMSI). We deduce that the extent of formation of exposed Pt peripheral sites with the TiO_2 support directly correlates with the activity of these Pt/TiO_2 catalysts.

Results

Hydrogenation of 3-nitrostyrene

Initially, a 0.2 wt.% Pt/TiO_2 catalyst reduced at 450 °C, was tested for the liquid phase hydrogenation of 3-nitrostyrene (3-NS) at 40 °C under 3 bar H_2 pressure with toluene as the solvent. 3-NS was rapidly and selectively converted into 3-VA; plots of 3-NS concentration versus time were linear up to about 25% conversion (SI, Fig. S1), giving an initial conversion rate of 1.55×10^{-3} mol_{3NS} L^{-1} min^{-1} with greater than 99% selectivity towards 3-vinylaniline (3-VA) (Figure 1(a)). Initial rates with different starting concentrations of 3-NS were used to confirm that reactions are zero order in 3-NS (SI, Figs. S2 & S3) for both 0.2 wt.% Pt/TiO_2 and 0.08 wt.% Pt/TiO_2. Other potential products such as (i) 3-ethyl nitrobenzene (3-ENB) formed by the selective hydrogenation of C=C and (ii) 3-ethylaniline (3-EA) formed by the complete hydrogenation of both the nitro and C=C groups were either not detected or were present only in trace quantities. In line with many other reports, the fully hydrogenated 3-ethyl-1-cyclohexylamine product was not detected under our reaction conditions; hence it is not included in the discussion (Scheme-1). Inspired by the work of Corma *et al.*[11], one portion of the dried-only 0.2 wt.% Pt/TiO_2 sample was calcined in static air at 450 °C for 4 h (*calc*) and a second portion was calcined at 450 °C for 4 h and then reduced using 5%H_2/Ar at 450 °C for 4 h (*calc+red*) and tested for the hydrogenation of 3-NS under identical reaction conditions. The 0.2 wt.% Pt/TiO_2 *calc+red* catalyst was found to be much more active (initial rate 6.04×10^{-3} mol_{3NS} L^{-1}

min^{-1}) compared to the 0.2 wt.% Pt/TiO$_2$ *red*-only catalyst. However, the selectivity to 3-VA for the *calc+red* catalyst was slightly lower (*ca.* 96%) compared to the *red*-only catalyst, because of the generation of the fully hydrogenated product (3-ethylaniline, 3-EA (4%)) (Figure S4). Corma *et al.*[11] reported that a 0.2 wt.% Pt/TiO$_2$ catalyst reduced at 450 $^{\circ}$C displayed the growth of a TiO$_2$ layer over the Pt nanoparticles resulting in a higher selectivity to 3-VA (*ca.* 90%). However, this same material reduced at 200 °C did not show any evidence of TiO$_x$ over-growth on the Pt nanoparticles and displayed a much lower selectivity for 3-VA (*ca.* 42%), with 3-EA (*ca.* 52%) being the main product.[11] In the present study, the 0.2% Pt/TiO$_2$ *red* and 0.2% Pt/TiO$_2$ *calc+red* materials, treated at 450 °C, showed a difference in their catalytic activities only (Figure 1), but not in their selectivities. In order to rationalise this observation, we prepared a series of Pt/TiO$_2$ catalysts with higher (0.5 wt.%) and lower (0.05 and 0.08 wt.%) Pt loadings. All these catalysts underwent reduction-only (*red*) or calcination-only (*calc*) or calcination followed by reduction (*calc+red*) heat treatments at 450 °C and were tested for the hydrogenation of 3-NS. The initial rates for all these catalysts are presented in Figure 1(a). For all the Pt loadings, the *calc*-only samples were found to be completely inactive and hence, for clarity, the data for these catalysts are not presented in Figures 1(a) & (b). For higher Pt loading catalysts (*i.e.,* 0.2 and 0.5 wt.%) the reaction rates of the *red*-only catalysts were found to be lower (1.55x10^{-3} mol$_{3NS}$ L^{-1} min^{-1} and 2.84x10^{-3} mol$_{3NS}$ L^{-1} min^{-1} respectively) compared to their counterpart *calc+red* catalysts (6.04x10^{-3} mol$_{3NS}$ L^{-1} min^{-1} and 1.11x10^{-2} mol$_{3NS}$ L^{-1} min^{-1} respectively). Interestingly, for the 0.05 wt.% Pt/TiO$_2$ catalyst, the opposite trend was observed whereby the *red*-only catalyst was found to be much more active (8.35x10^{-4} mol$_{3NS}$ L^{-1} min^{-1}) compared to the *calc+red* catalyst (1.59x10^{-4} mol$_{3NS}$ L^{-1} min^{-1}) under identical reaction conditions. However, for the 0.08 wt.% Pt/TiO$_2$ catalyst the *red* and the *calc+red* samples displayed similar activity levels (*i.e.,* 1.75x10^{-3} mol$_{3NS}$ L^{-1} min^{-1} and 1.78x10^{-3} mol$_{3NS}$ L^{-1} min^{-1} respectively). It is important to highlight that

for all catalysts, irrespective of Pt loading or heat treatment protocol, the selectivity to 3-VA remained very high (> 90 %). It should also be noted that the catalysts with higher Pt loadings (*i.e.,* 0.2 and 0.5 wt.%) subjected to the *calc+red* treatment showed slightly lower selectivity (because of the production of some 3-EA, which is an over hydrogenation product) as compared to the corresponding *red*-only samples (see 3-VA selectivity versus 3-NS conversion plot in Figure S4). These results demonstrate that the post-synthesis heat treatment protocols combined with the Pt loading modulate the active sites for this chemoselective hydrogenation reaction. The initial rate data of all the *red* and *calc+red* Pt/TiO$_2$ samples with different metal loadings are reported in SI, Figure S1.
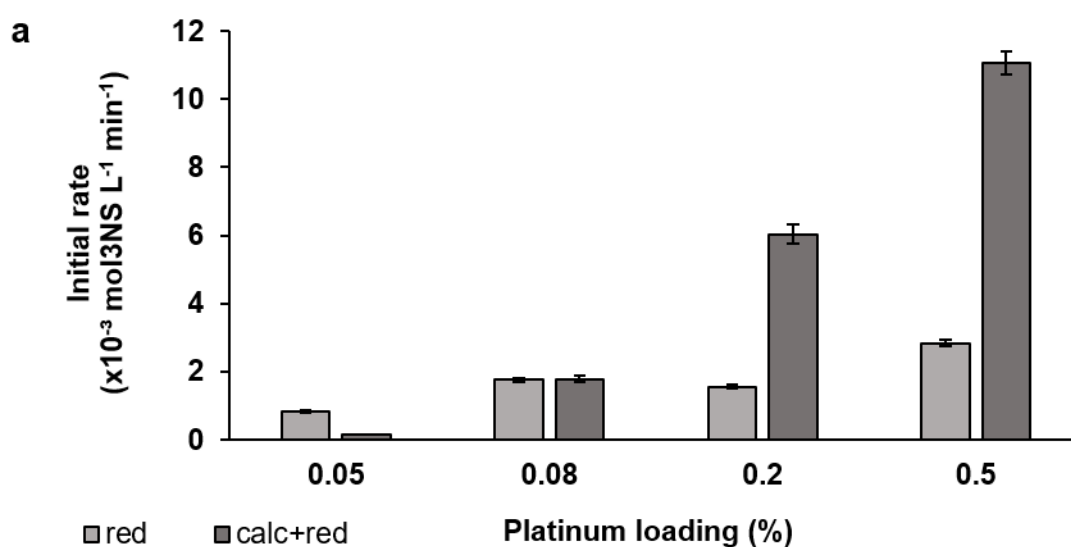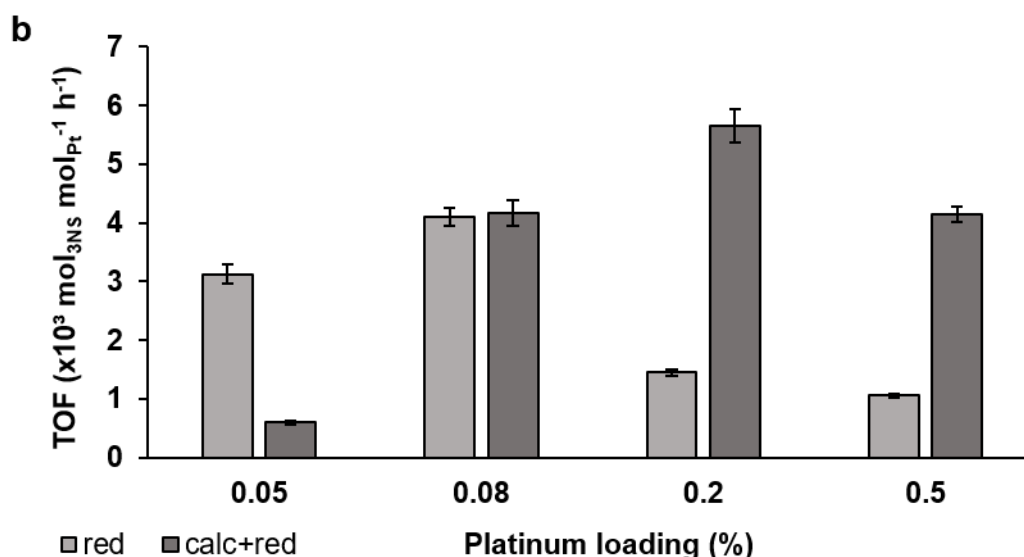
Figure 1: Effect of different heat treatments (i.e., red versus calc+red) on the activity of Pt/TiO$_2$ catalysts having different (i.e., 0.05, 0.08, 0.2, 0.5 wt.%) Pt loadings. (a) Initial 3-NS conversion rates; (b) Turnover frequencies (TOF) based on the initial rate obtained during the selective hydrogenation of 3-NS. Reaction conditions: 3-NS: 0.2 ml; toluene: 8ml; pH$_2$: 3bar; catalyst: 50 mg; temperature: 40 °C.
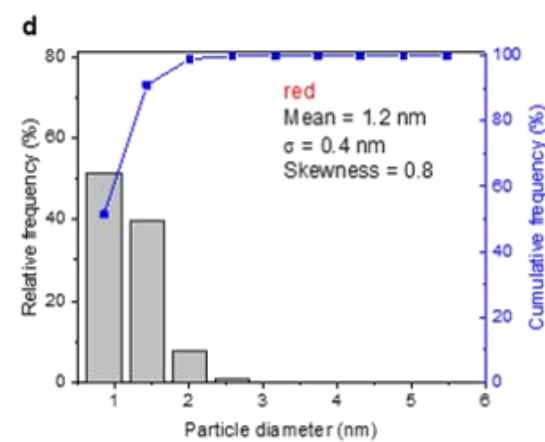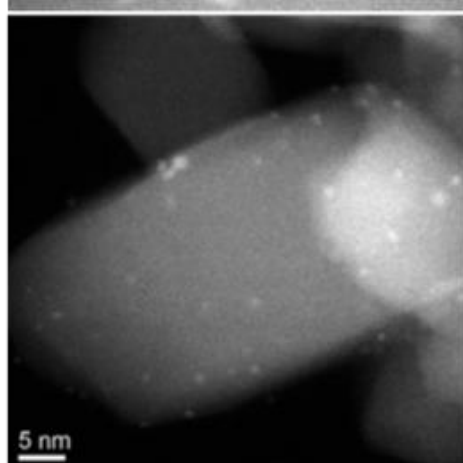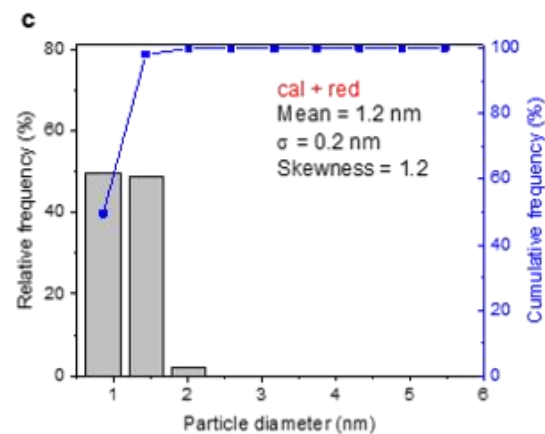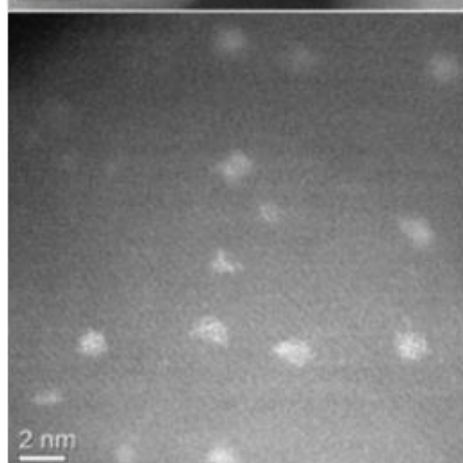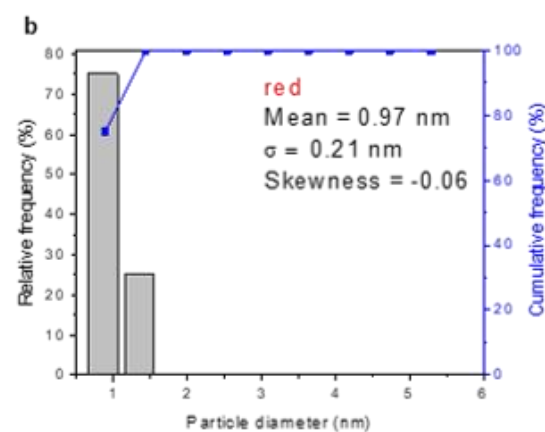
Since the catalysts have different Pt loadings, their conversion rates were normalised using the Pt loadings to allow for a meaningful comparison of their catalytic activities. The resultant TOFs (Figure 1(b)) shows an exceptional intrinsic activity of the 0.2 wt.% Pt/TiO$_2$ *calc+red* catalyst (5650 mol$_{3NS}$ mol$_{Pt}^{-1}$ h^{-1}). Comparing this TOF value with other reported literature values (SI, Table S1) it is clear that our 0.2 wt.% Pt/TiO$_2$ *calc+red* material is the most active catalyst reported to date under comparable reaction conditions. It should be noted that much higher TOFs have been reported under harsher reaction conditions (*i.e,* higher temperatures, greater H$_2$ pressure and higher metal loadings).[29,30] In an effort to unravel the relationship

between metal loading, heat treatment protocol and the nanostructural properties of these catalysts, all these materials were comprehensively characterised using a complementary set of *state-of-the-art* microscopic and spectroscopic methods.

Electron microscopy studies

Figure 2 shows some representative HAADF-STEM images of *red* and *calc+red* samples of Pt/TiO_2 catalysts with different Pt loadings (*i.e.,* 0.05, 0.08, 0.2 and 0.5 wt.%). The corresponding images of the *calc* series of samples are presented in SI, Figure S5. This study allowed us to follow how the size and structure of the Pt nanoparticles changes according to the heat treatment applied for each Pt loading level. In all the *calc*-only samples, the vast majority of the Pt species are sub-nm clusters and highly dispersed single Pt atoms distributed over the support (SI, Figure S5). In the 0.05 wt.% Pt/TiO_2 catalyst (Figures 2 (a) and (b)), the Pt particles found in both the *red*-only and the *calc+red* were ultra-small clusters, however single Pt atoms were not detected. The *red*-only sample had a more uniform particle size distribution as compared to the *calc+red* catalyst, which correlates well with the observed catalytic activity trend. In the case of the 0.08 wt.% Pt/TiO_2 material (Figures 2(c) and (d)), both *red*-only and *calc+red* samples possess a very similar nanostructure with a uniformly small mean Pt particle size (1-2 nm) and reasonably similar particle size distributions. This observation again correlates well with the very similar catalytic activities noted for the *red*-only and *calc+red* samples of the 0.08 wt.% Pt/TiO_2 catalyst (Figure 1). In the case of 0.2 wt.% Pt/TiO_2 catalyst (Figures 2(e) and (f)), the *calc+red* sample showed many uniformly distributed small Pt particles (1-2 nm) distributed over the TiO_2 support. However, the corresponding *red*-only sample showed a wider distribution of Pt particle sizes (1-4 nm) with a larger mean particle

diameter (1.6 nm). In the case of the 0.5 wt.% Pt/TiO_2 catalyst (Figures 2(g) and 2(h)), the *red*-only sample showed a mixture of smaller particles (*ca.* 1-2 nm) and larger particles (>5 nm), whereas in the corresponding *calc+red* variant, uniform particles are homogeneously distributed over the TiO_2 surface. The possibility of improving the metal dispersion in favour of small Pt particles by performing consecutive calcination and reduction treatments has been observed before.[26,27] Our microstructural observations correlate very well with the measured catalytic activites for these various Pt/TiO_2 catalysts, indicating that smaller Pt particles with high dispersion and narrow size distribution lead to a higher overall catalytic activity. Analysis of the particle size distribution data for all the samples in this study (Figure 2) reveals that those Pt/TiO_2 catalysts having the largest population of ~1 nm particles and narrowest size distribution (*i.e.,* 0.08 wt.% Pt/TiO_2 (*red*), 0.08 wt.% Pt/TiO_2 (*calc+red*) and 0.2 wt.% Pt/TiO_2 (*calc+red*)) also showed the highest catalytic activity in terms of TOF values (Figure 1(b)).

a
cal + red
Mean = 1.18 nm
σ = 0.3 nm
Skewness = 0.03

b
red
Mean = 0.97 nm
σ = 0.21 nm
Skewness = -0.06

c
cal + red
Mean = 1.2 nm
σ = 0.2 nm
Skewness = 1.2

d
red
Mean = 1.2 nm
σ = 0.4 nm
Skewness = 0.8

e

cal + red
Mean = 1.1 nm
σ = 0.2 nm
Skewness = 0.5

f

red
Mean = 1.6 nm
σ = 0.6 nm
Skewness = 0.4

g

calc + red
Mean = 1.4 nm
σ = 0.2 nm
Skewness = 0.5

h

red
Mean = 1.6 nm
σ = 0.6 nm
Skewness = 0.6
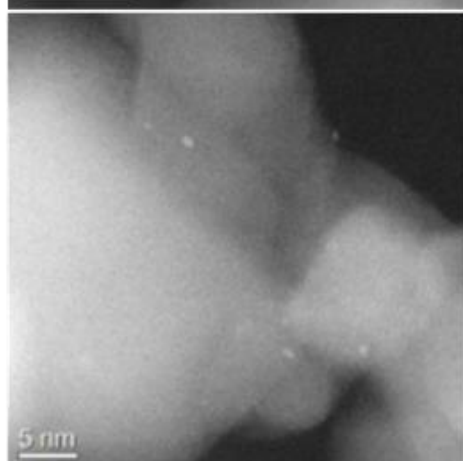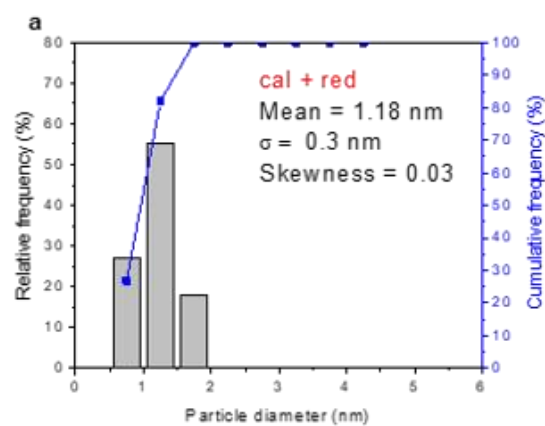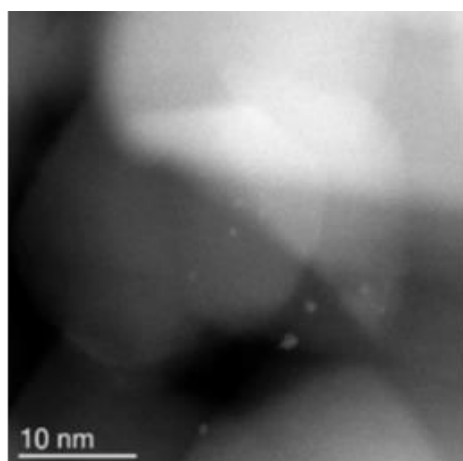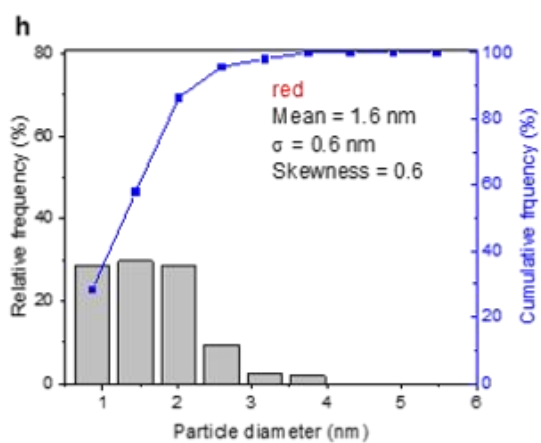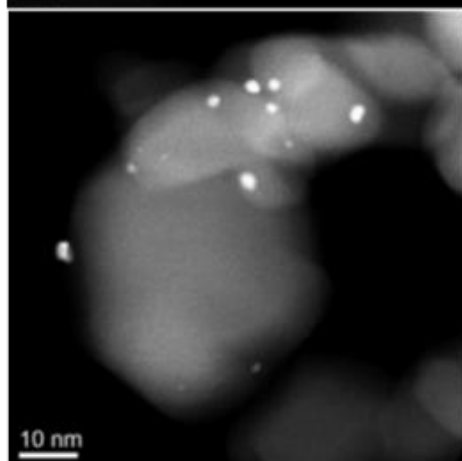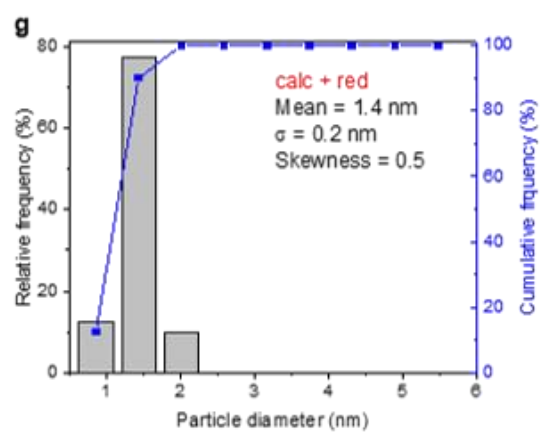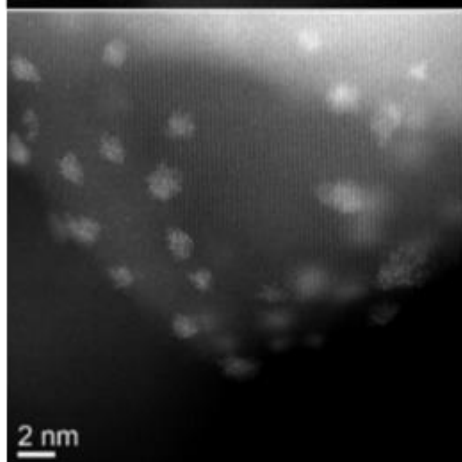
Figure 2: *Representative HAADF-STEM images and the derived particle size distributions of the unused Pt/TiO₂ catalysts; (a) 0.05 wt.% Pt/TiO₂ (calc+red), (b) 0.05 wt.% Pt/TiO₂ (red), (c) 0.08 wt.% Pt/TiO₂ (calc+red), (d) 0.08 wt.% Pt/TiO₂ (red), (e) 0.2 wt.% Pt/TiO₂ (calc+red), (f) 0.2 wt.% Pt/TiO₂ (red), (g) 0.5 wt.% Pt/TiO₂ (calc+red) and (h) 0.5 wt.% Pt/TiO₂ (red).*

X-ray photoelectron spectroscopy studies

All the Pt/TiO₂ catalysts with different loadings and heat treatment protocols were characterised by XPS and the results are shown in Figure 3. It should be noted that the samples with very low loading levels (*i.e.,* < 0.1wt.%) , gave noisy spectra even after an unusually large number of scans (>100). This signal-to-noise ratio problem was compounded by the presence of an overlapping Ti loss peak at *ca.* 75 eV which made quantification of these particular spectra quite challenging.[28]

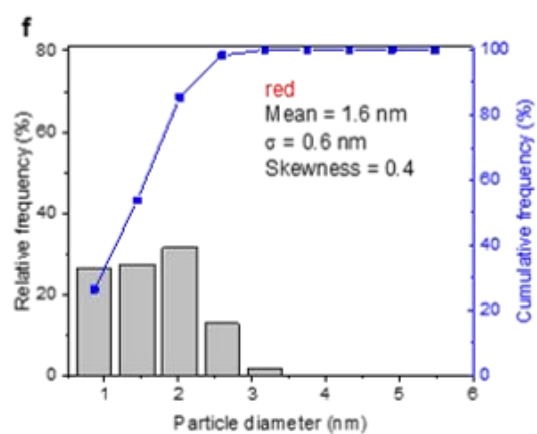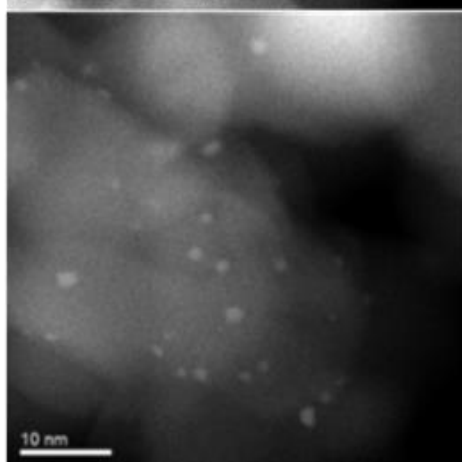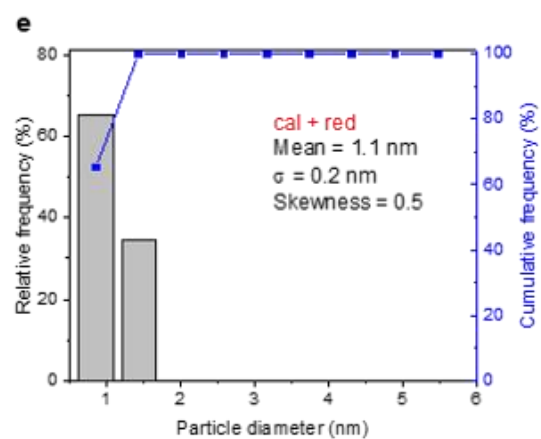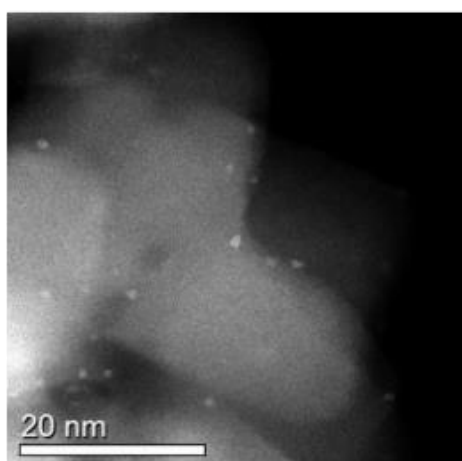Generally, regardless of Pt loading, the XPS data were quite similar, therefore for conciseness of discussion we will focus initially on the data acquitred from the 0.5 wt.% Pt/TiO₂ catalysts. For the dried-only sample, a Pt($4f_{7/2}$) binding energy of 72.2 eV was measured, which is indicative of a Pt(II) species, presumably associated with residual chlorine as detected by XPS, although the presence of Pt oxides cannot be excluded.[29,30] Calcination of this highest loading sample revealed two distinct Pt environments; the first with a binding energy again of 72.2 eV and a second with a binding energy of 74.4 eV. Considering the calcination temperature employed (450 °C), the small concentration of Cl detected (*ca.* $0.2 - 0.25$ at.%, see SI, Table S2), and the nominal Pt concentration (*ca.* 0.2 at.%, see SI, Table S2) a bulk $PtCl_2$ species is not the cause of the 72.2 eV signal, therefore this is likely a PtO_x phase. The higher binding energy component at 74.4 eV, can be assigned as PtO_2 or Pt hydroxide.[31]

Both '*red*' and '*calc + red*' catalysts exhibit Pt(0), as indicated by the asymmetric peak shape and a binding energy of 70.6 – 70.8 eV.[32] Representative HAADF-STEM lattice images of the 0.5 wt.% Pt/TiO$_2$ (*red*), (presented in SI, Figure S6), confirms the presence of metallic Pt(0) structure in larger particles.
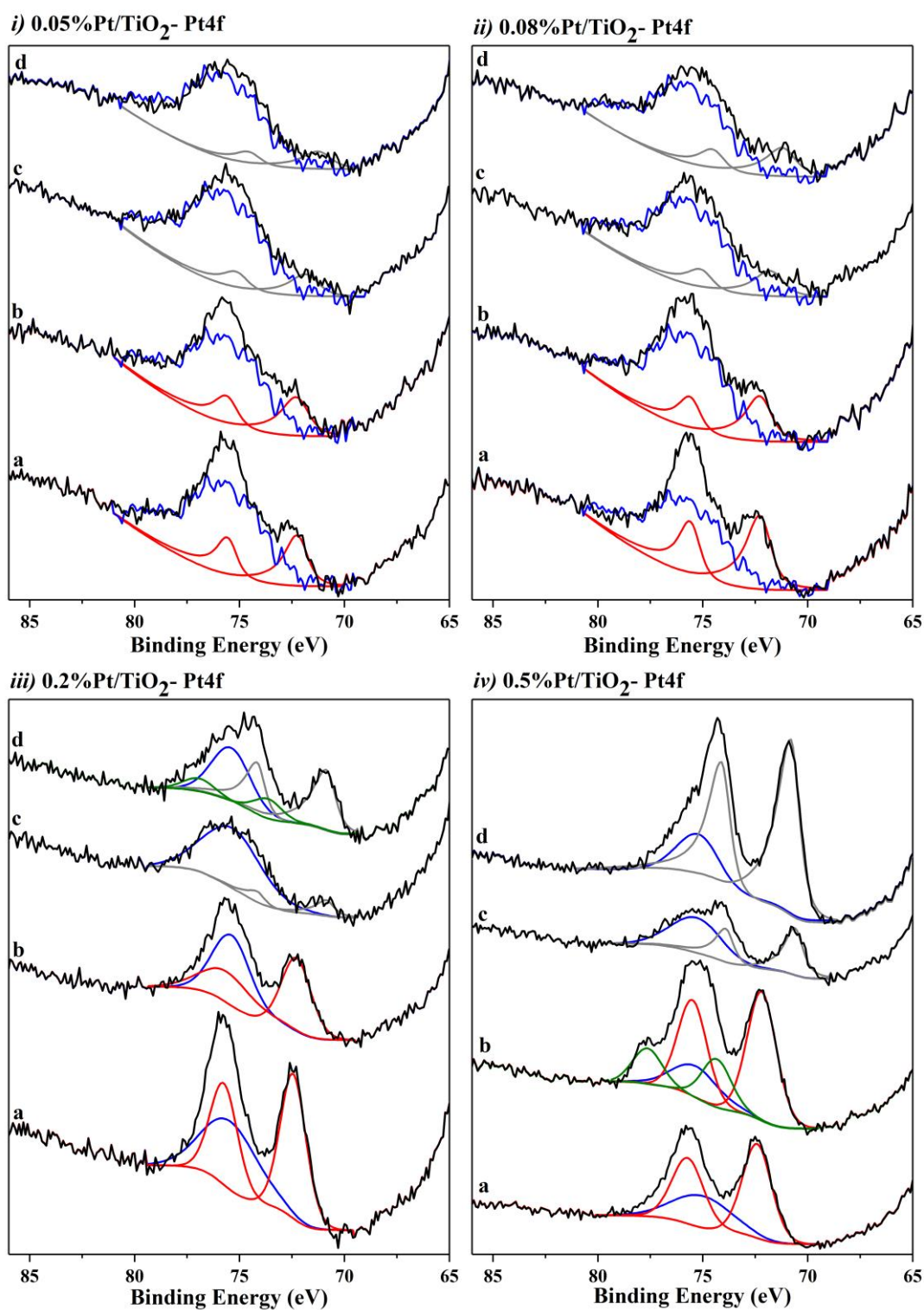
Figure 3: XPS data of the (a) dried only, (b), calcined-only, (c) reduced-only and (d) calcined+reduced Pt/TiO₂ catalysts with different Pt loading levels (i.e., (i) 0.05 wt.%; (ii) 0.08 wt.%; (iii)0.2 wt.%; (iv) 0.5 wt.%).

For the low (0.08 and 0.05 wt.%) Pt loading catalysts, depending on the heat treatments, the Pt(4f) signal strength was very weak, especially for those materials that had undergone reductive treatments, which is attributed to changes in the particle size.

X-ray absorption spectroscopy studies

XAFS measurements were performed for the 0.05, 0.08, 0.2 and 0.5 wt.% Pt/TiO$_2$ (*red & calc+red*) samples. Analysis of the XAFS data included interpretation of both XANES and EXAFS information. The platinum L$_3$ edge XANES spectrum is dominated by the dipole allowed $2p_{3/2} \rightarrow 5d_{5/2}$ transition of a core electron, which is known to be sensitive to the oxidation and co-ordination state of Pt.[33-36] In Figures 4 (a) and (b), the XANES plots show a comparison of samples with different metal loadings that underwent the same heat treatment: namely *red*-only (Figure 4(a)) or *calc+red* (Figure 4(b)). Figure S7 also contains a plot of the XANES for the 0.05 wt.% Pt/TiO$_2$ samples and the PtO$_2$ reference material. Already from this overview it is possible to notice the variety of platinum species and environments present in these samples.
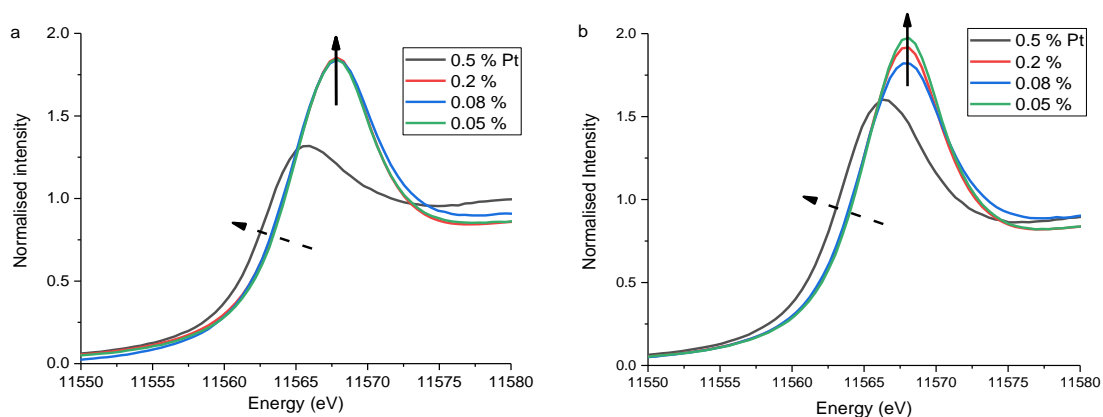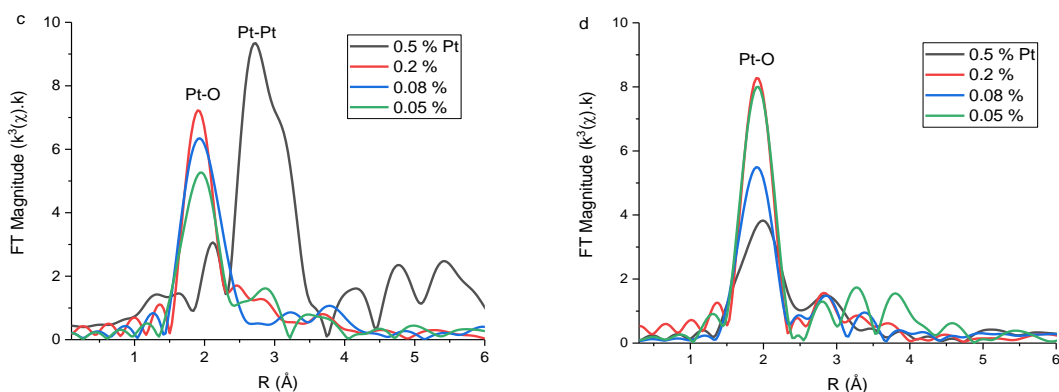
Figure 4. *Pt L$_3$-edge XANES (a and b) and k^3 EXAFS FT (c and d) data recorded on Pt/TiO$_2$ samples after reduction only (a, c) and calcination + reduction (b, d). Note: dashed arrow indicates the decrease in edge position with increased loading. The solid arrow indicates the increased rising absorption edge. Labels above the peaks indicate the scattering pairs that give rise to that contribution.*

The XANES spectra in Figure 4(a) appear almost identical for the three lowest Pt loadings (*i.e.,* 0.05, 0.08 and 0.2 wt.%) with a maximum in the μ(E) trace seen at ~ 11,568 eV. It is noticeable however that the maximum of the rising absorption edge of the samples and the edge position is lower (*i.e.,* 'red'-shifted) compared that of the reference PtO$_2$ phase (Figure S7). The sample with 0.5 wt.% Pt loading is especially red-shifted and its rising absorption edge possesses the lowest overall intensity, particularly at 11,568 eV. Previously it has been shown that such changes indicate differences in the extent of reduction/oxidation with all samples possessing an average Pt oxidation state $< +4$ with the 0.5 wt.% sample being more reduced than all samples with lower loadings, which are seen to be the most oxidised.[37] These

observations are entirely consistent with the XPS and HAADF-STEM data shown in Figures 3 and S6 respectively.

A similar situation can be seen for the *calc+red* samples shown in Figure 4(b), although, based on the intensity of the rising absorption edge, all samples except that containing 0.08 wt.% Pt appear more oxidised than after simple reduction; the 0.08 wt.% sample appearing to remain the same. In order to verify and even extract further information from these samples, the EXAFS Fourier Transform (FT) data are plotted in Figures 4 (c) and (d). Focusing on Figure 4(c) of the *reduced*-only samples, it is clear that all except the 0.5 wt.% Pt/TiO$_2$ *red* sample contain a strong peak at ~ 2.0 Å assignable to a Pt-O distance typical of PtO$_2$ species; see Figure S8(a) which illustrates the similarities of the Pt-O distances in these samples compared to that of PtO$_2$.[38,39] The intensity of the Pt-O contribution with respect to the reference PtO$_2$ is much smaller in all the reduced samples and suggests that the Pt-O environments in the samples are more disordered. This can be rationalised as due to static disorder caused by the high dispersion of PtO$_2$ species across the TiO$_2$ support and according to the XANES, a partial reduction of the Pt^{4+} to Pt^{2+}. Note that since a PtO reference is not readily available, it is not possible to unambiguously identify its presence nor rule out its absence. The 0.5 wt.% Pt/TiO$_2$ *red*-only sample also contains a broad peak with a maximum intensity at ~ 2.73 Å typical of Pt metal. Analysis of the EXAFS data (see Figure S9 and Table S3) for this sample suggests the existence of Pt nanoparticles ~ 1 nm in diameter.[40] For the 0.05 and 0.2 wt.% Pt/TiO$_2$ *red*-only samples, weak peaks at 2.87 and 2.81 Å may also suggest the presence of a small amount of Pt metal in these samples, as well as a much more significant Pt-oxide environment.

Figure 4(d) contains FT data of the corresponding *calc+red* samples and are characterised by the presence of a strong Pt-O contribution in all samples, although the intensity of this contribution is inversely proportional to the amount of Pt present; see Figure S8(b) which illustrates the similarities of the Pt-O distances in the samples to that of the reference PtO_2 material. This is again consistent with the XANES data, which suggests the presence of more Pt^{4+} in the samples after the *calc+red* treatment; the 0.05 wt.% Pt/TiO_2 *calc+red* sample in particular contains Pt-Pt scattering contributions consistent with PtO_2 suggesting that in this sample some PtO_2 nanocrystallites may have evolved. For the 0.5 wt% Pt/TiO_2 *calc+red* sample, the Pt-O peak possesses a skew and kurtosis towards higher Pt-O distances and when considered along with the weaker absorption edge intensity for this sample, suggests the presence of more Pt^{2+}. Interestingly no real evidence for metallic Pt species could be seen on visual inspection or when attempts were made to fit the data.

CO DRIFTS analysis

CO DRIFTS analysis was performed on all of the Pt/TiO_2 catalysts to gain an accurate measure of the degree of Pt metal exposure on the surface of the catalysts. For all the samples, a broad asymmetric band was observed between $2050 - 2060$ cm^{-1} and for all the *calc+red* samples, a sharp band at *ca.* 2089 cm^{-1} was also present (Figure 5). It has been reported that the band at *ca.* 2050-2060 cm^{-1} corresponds to CO linearly adsorbed on low coordination Pt edge and corner sites.[11,41-44] This IR band is quite sensitive to a number of factors including Pt dispersion, Pt microstructure (*i.e.,* steps, crystal face, *etc.*) and charge transfer in the vicinity of the Pt adsorption site. The band at *ca.* 2089 cm^{-1} corresponds to CO molecules adsorbed on Pt (111) terrace sites having a coordination number of 9.[11,43-45] The Pt/TiO_2 system has also been widely

reported to display a strong metal support interaction (SMSI), especially when reduced at temperatures higher than 400 °C, which typically results in a much lower uptake or adsorption of CO.[46] The 0.5 wt.% Pt/TiO_2 *red*-only and 0.2 wt.% Pt/TiO_2 *red*-only samples exhibit substantially less CO adsorption confirming the presence of an SMSI effect in these samples. The SMSI could be associated with the formation of bonds between Pt metal and *cationic* or *atomic* Ti species or by coverage of the platinum particle by a layer of TiO_x, as a result of hydrogen spill-over. Corma *et al.* has reported TiO_2 coverage over Pt particles for a 0.2 wt.% Pt/TiO_2 sample reduced at 450 °C.[11] Combining our CO DRIFTS data with reported interpretations, we consider that the Pt nanoparticles are covered by TiO_x for the 0.5 wt.% Pt/TiO_2 *red*-only and 0.2 wt.% Pt/TiO_2 *red*-only samples, even though this layer was not resolved by STEM. Analysing the TOF values of these two samples from Figure 1, it is clear that their activities are much lower than all of the other samples tested (1060 mol_{3NS} mol_{Pt}^{-1} h^{-1} and 1450 mol_{3NS} mol_{Pt}^{-1} h^{-1}, respectively). Although some SMSI effect can be beneficial for increasing chemoselectivity in this reaction, an excessive TiO_x overlayer on the Pt can be detrimental to the overall catalytic activity through complete site blocking. For the 0.5 wt.% Pt/TiO_2 and 0.2 wt.% Pt/TiO_2 catalysts subjected to the *calc+red* treatment, the Pt particles were not completely covered by TiO_x leaving some Pt sites exposed for catalytic turnover. Although we could not directly visualise the surface coverage of Pt nanoparticles by TiO_x, CO DRIFTS data provides convincing evidence for some TiO_x coverage of Pt particles in the 0.5 wt.% Pt/TiO_2 and 0.2 wt.% Pt/TiO_2 *red*-only samples.
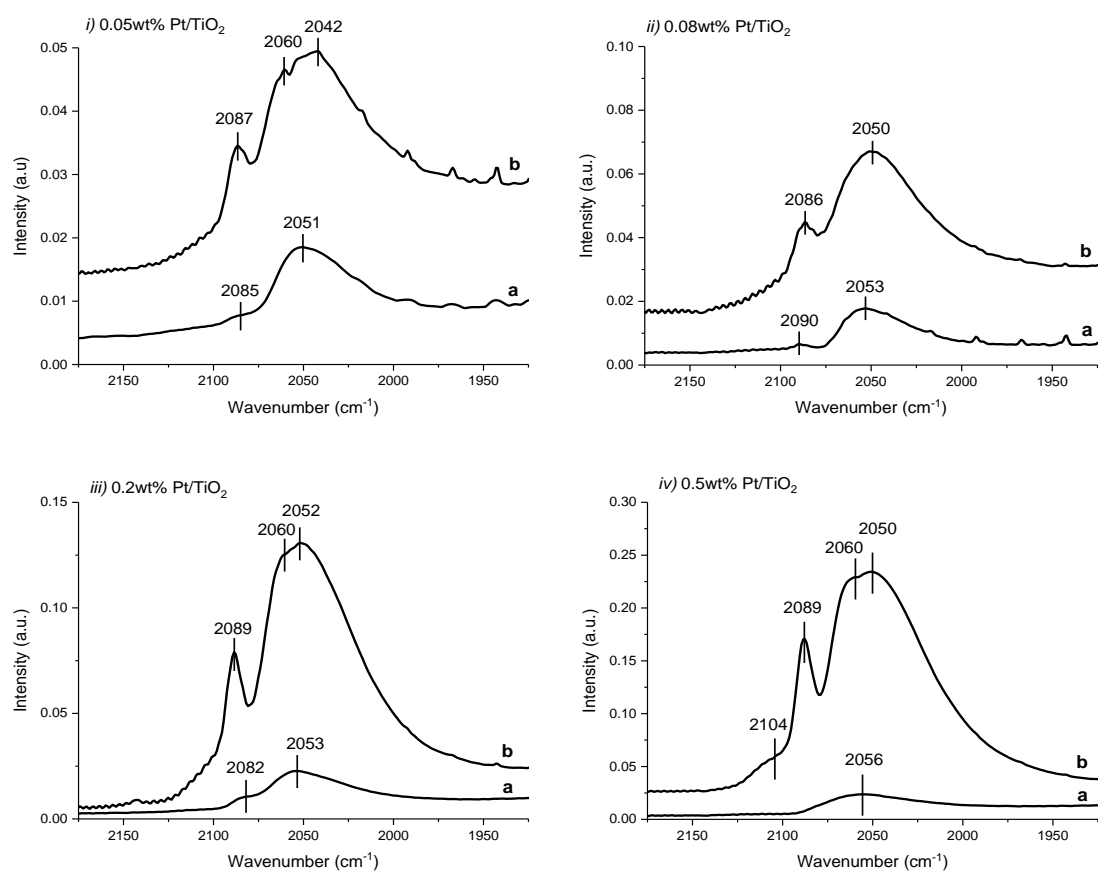
Figure 5. *CO DRIFTS spectra of the (i) 0.05 wt.%, (ii), 0.08 wt.%, (iii), 0.2 wt.% and (iv) 0.5 wt.% Pt/TiO₂ catalysts in (a) the reduced only and (b) calcined + reduced states.*

It has previously been reported that peripheral sites at the Pt/TiO$_2$ interface are important for some selective hydrogenation reactions such as the hydrogenation of crotonaldehyde and furfuraldehyde.[47,48] Following this observation, the total number of peripheral sites for all the Pt/TiO$_2$ catalysts examined were estimated by assuming all Pt particles are half-'sphere' Mackay icosahedra (see SI, Table S4), based on the particle size distributions derived from HAADF-STEM images. The total number of Pt peripheral sites, expressed as a weight percentage of the total catalyst mass, for the various Pt/TiO$_2$ materials, are plotted in Figure 6(a) together with the 3-NS initial conversion rate.

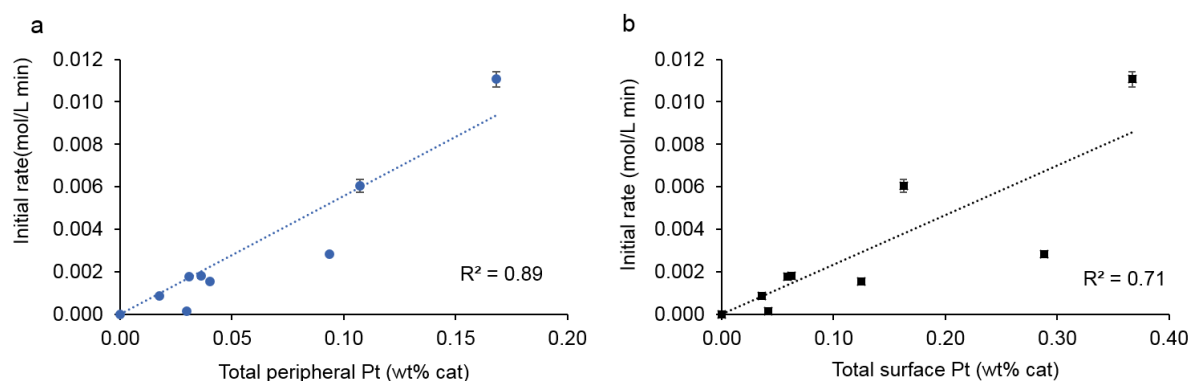*Figure 6*. *The correlation between the 3-NS initial conversion rate and total amount of Pt present in (a) peripheral sites and (b) as exposed surface atoms for the different Pt/TiO$_2$ catalysts as estimated from analysis of HAADF-STEM images. For model (a) R^2 = 0.89, p<0.001, and for model (b) R^2 = 0.71, p<0.02.*

A highly significant positive correlation is observed between the number of peripheral Pt sites and catalytic activity (Figure 6(a)), supporting the proposition of Boronat *et al.* that the peripheral sites created where the Pt nanoparticles make contact with the TiO$_2$ support are very important for the selective hydrogenation of nitrogroups.[49] A weaker fit is observed when the same initial rate data was plotted against the total number of exposed surface Pt atoms (Figure 6(b)). The Pt surface area determined through CO chemisorption was plotted against the initial rate (SI, Figure S11) also gave a weaker correlation. These data from two different methods indicate that the Pt surface atoms may not be the active sites. Post synthetic heat treatment plays an important role in inducing SMSI effects in Pt/TiO$_2$ catalysts, which in turn has a profound impact on their resultant catalytic activities. High temperature reduction induces coverage of Pt sites by TiO$_x$. This problem can be eliminated however by employing a sequential calcination step followed by reduction step. We propose that the calcination step prior to the reduction treatment more effectively anchors the Pt particles to the support and thus limits their subsequent mobility during the reduction

treatment. From the particle size distribution data (Figure 2), it is evident that, among all the catalysts tested, only 0.5wt%Pt/TiO$_2$ – *red* & 0.2 wt.% Pt/TiO$_2$ – *red* samples have metal particles larger than 2-3 nm. From CO-DRIFTS data (Figure 5), only these two samples show signs of TiOx coverage over Pt particles. This suggest a possible size dependant TiOx coverage phenomenon which needs further detailed investigation. With the current data we conclude that for samples with higher Pt loadings, a *calcination+reduction* treatment results in more active catalysts compared to *reduced*-only catalysts. In the case of lower Pt loadings, due to high dispersion and relative scarcity of nearby Pt neighbours, even with a reduction-only treatment, there is little agglomeration of the Pt nanoparticles in spite of Pt mobility. Hence, the calcination pre-step is not necessary for samples with low Pt loadings. The collective electron microscopy and spectroscopic data obtained from all the Pt/TiO$_2$ samples suggests that those materials with very small Pt particles (~ 1 nm) and without any significant TiO$_x$ surface coverage display exceptional catalytic performance.

Conclusions

Pt nanoparticles supported on TiO$_2$ with different Pt loadings, were found to be remarkably active and selective for the chemoselective hydrogenation of 3-NS to 3-VA. Amongst all the catalysts tested, the 0.2 wt.% Pt/TiO$_2$ *calc+red* material was found to be the most active. It was also the catalyst with the highest number of peripheral active sites generated as a result of the combination of ultra-small Pt nanoparticles (~1 nm) with a tight particle size distribution in which the the Pt particles were not covered by TiO$_x$. This nanostructure was achieved by combining a calcination treatment at 450 °C with a subsequent reduction of this catalyst at 450 °C, thereby preventing any TiO$_x$ coverage of the Pt active sites. For the same 0.2 wt.%

level of Pt loading, a reduction treatment alone at 450 °C induces an SMSI effect which results in the partial coverage of active Pt sites and a less active catalyst.

Methods

Catalyst Preparation

Supported Pt catalysts with different Pt loadings (0.05, 0.08, 0.2 and 0.5 wt.%) were synthesised using a wet-impregnation method. The dried materials were then heat treated in a number of ways and tested for the chemoselective hydrogenation of 3-nitrostyrene. For a typical catalyst preparation (2g), the requisite amount of aqueous hydrogen hexachloroplatinic acid solution (9.6 mg Pt/ml, assay 30.21% H_2PtCl_6, Johnson Matthey) was diluted to 16 ml using deionised water and heated in an oil bath to 60 °C with vigorous stirring (800 rpm) before addition of the requisite amount of support (TiO_2, Evonik®P25). The temperature was then increased to 95 °C for 16 h to dry the slurry in air. The resultant material was then ground thoroughly (designated as 'fresh dried-only' sample). A portion (500 mg) of the dried-only sample was either calcined in static air or reduced under a steady flow of 5% H_2/Ar. Heat treatments were carried out at 450 °C for 4 h with a heating rate of 10 °C min^{-1}. Samples that underwent reduction-only were denoted as "*red*", calcination only as "*calc*" and calcination followed by reduction treatment as "*calc+red*". All these materials were tested as catalysts without any further treatment unless stated otherwise.

Hydrogenation of 3-nitrostyrene

Liquid phase chemoselective hydrogenation of 3-nitrostyrene was performed in a 50 ml glass round bottom Colaver® reactor. In a typical reaction, 3-nitrostyrene (0.2 ml), toluene (8 ml) and catalyst (50 mg) were charged in the reactor which was then purged with N_2 to remove traces of air and immersed in an oil bath set at 40 °C. After purging the reactor three times with 3 bar H_2 while stirring, the reaction was

commenced. After a pre-determined reaction time, the reactor was cooled to <5 °C using ice, after which aliquots of the reaction mixture were collected and centrifuged to remove the solid catalyst. The liquid reaction mixture (1 ml) was added to a GC vial together with a fixed amount of external standard o-xylene (0.1 ml) for further quantitative analysis. The determination of the conversion was performed using a Varian 450GC Gas Chromatograph equipped with a HP-5ms boiling point column, a Flame Ionisation detector (FID) and a CP8400 Autosampler. Conversion of the substrate and product selectivity were calculated using suitable calibration plots and response factors.

Catalyst Characterization

X-ray Photoelectron Spectroscopy (XPS)

XPS was performed using two systems; the first was a Kratos Axis Ultra DLD spectrometer using monochromatic Al Kα radiation (source power 140 W). An analyser pass energy of 160 eV was used for survey scans, and 40 eV for detailed acquisition of individual elemental regions. The second system was a Thermo Scientific K-Alpha$^+$ spectrometer utilizing microsfocused monochromatic Al Kα radiation (source power 72 W), with analyser pass energies of 40 and 150 eV. Data was analysed with CasaXPS, using escape depth corrected sensitivity factors supplied by the instrument manufacturers.

Scanning Transmission Electron Microscopy

Samples for examination by STEM were prepared by dry dispersion of the catalyst powder onto a holey carbon film supported by a 300 mesh copper TEM grid. Bright field (BF) and high angle annular dark field (HAADF) STEM images were taken using an aberration corrected JEM ARM-200CF microscope operating at 200kV. This instrument was also equipped with a JEOL Centurio silicon drift detector for X-ray

energy dispersive spectroscopy (XEDS). Particle size distribution analysis was performed from analysis of HAADF electron micrographs using Image J.

X-ray Absorption Spectroscopy

XAFS spectroscopy measurements were performed on stations B18 and I20 at the Diamond Light Source (Harwell, Oxon) operating at 3 GeV in multibunch mode with a current of 200 mA. Both stations are equipped with a Si(111) double crystal monochromator, ion chambers for measuring incident and transmitted beam intensities and/or a multi-element Ge (fluorescence) detector for recording X-ray absorption spectra. The measurements were carried out in air on self-supporting wafers (approximately 100 mg) at the Pt L_3 edge, and a 10 µm thick Pt foil was used as a calibration sample for the monochromator. Measurements were performed at room temperature in normal step scanning mode. To improve the signal-to-noise ratio, multiple scans were taken. All data were subjected to background correction using Athena (*i.e.,* IFEFFIT software package for pre- and post-edge background subtraction and data normalisation). XAFS spectra were normalized from 30 to 150 eV above the edge energy, while the EXAFS spectra were normalized from 150 eV to the last data point using the Autobk algorithm. Normalisation was performed between $\mu(E)$ and $\mu_0(E)$ via a line regression through the data in the region below the edge and subtracted from the data. A quadratic polynomial was then regressed to the data above the edge and extrapolated back to E_0. The extrapolated value of the post edge polynomial at E_0 was used as the normalisation constant. This threshold energy (E_0) is normally determined using either the maximum in the 1st derivative, approximately 50 % of the rising absorption edge, or immediately after any pre-edge or shoulder features. The isolated EXAFS spectra were analysed using the DL-EXCURV programme. Data was analysed using a least squares single or dual shell EXAFS

fitting analysis performed on data that had been phase corrected using muffin-tin potentials. Amplitude reduction factors (S_o^2) of 0.94 obtained from fitting a Pt metal foil, was also used in the analysis.

CO DRIFTS

For CO-DRIFTS analysis, samples were loaded in a DRIFT Tensor 27 spectrometer, and flushed with N_2 for 30 min to record a baseline. The sample was then exposed to 20% CO/Ar until complete saturation of the Pt sites was achieved. The system was then flushed with pure N_2 until there was no presence of atmospheric CO and then the spectra were recorded.

Authors contribution:

MM, AJB and RQ performed the catalyst preparation and catalyst testing under the supervision of MS, ND, SF and XG. SMA, QH and CJK carried out electron microscopy studies of the catalyst. DJM performed the XPS characterisation of the catalysts. EG and AMB analysed the XAS data. DB suggested the kinetics experiments presented in this article. MS conceived this idea and supervised the project. GJH directed this project. All authors contributed to the data analysis and drafting of this manuscript.

Competing interests

The authors declare no competing financial interests.

References

1   Wang, L. *et al.* Single-site catalyst promoters accelerate metal-catalyzed nitroarene hydrogenation. *Nature Communications* **9**, 1362, (2018).

2   Therrien, A. J. *et al.* An atomic-scale view of single-site Pt catalysis for low-temperature CO oxidation. *Nature Catalysis* **1**, 192-198, (2018).

3   Vile, G., Albani, D., Almora-Barrios, N., Lopez, N. & Perez-Ramirez, J. Advances in the design of nanostructured catalysts for selective hydrogenation. *Chem.Cat.Chem.* **8**, 21-33, (2016).

4   Blaser, H. U., Steiner, H. & Studer, M. Selective catalytic hydrogenation of functionalized nitroarenes: An update. *Chem.Cat.Chem.* **1**, 210-221, (2009).

5   Song, J. J. *et al.* Review on selective hydrogenation of nitroarene by catalytic, photocatalytic and electrocatalytic reactions. *Applied Catalysis B - Environmental* **227**, 386-408, (2018).

6   Rylander, P. N. *Hydrogenation Methods*. (Academic Press, 1990).

7   Nishimura, S. *Handbook of Heterogeneous Catalytic Hydrogenation for Organic Synthesis* (Wiley-VCH, 2001).

8   Bellamy, F. D. & Ou, K. Selective reduction of aromatic nitro-compounds with stannous chloride in non-acidic and non-aqueous medium. *Tetrahedron Letters* **25**, 839-842, (1984).

9   Basu, M. K., Becker, F. F. & Banik, B. K. Ultrasound-promoted highly efficient reduction of aromatic nitro compounds to the aromatic amines by samarium/ammonium chloride. *Tetrahedron Letters* **41**, 5603-5606, (2000).

10   Burawoy, A. & Critchley, J. P. Electronic spectra of organic molecules and their interpretation-V*. *Tetrahedron* **5**, 340-351, (1959).

11   Corma, A., Serna, P., Concepcion, P. & Calvino, J. J. Transforming non-selective into chemoselective metal catalysts for the hydrogenation of substituted nitroaromatics. *Journal of the American Chemical Society* **130**, 8748-8753, (2008).

12   Arnold, H., Döbert, F. & Gaube, J. in *Handbook of Heterogeneous Catalysis* (Wiley-VCH, 2008).

13   Shi, Q. X., Lu, R. W., Jin, K., Zhang, Z. X. & Zhao, D. F. Simple and eco-friendly reduction of nitroarenes to the corresponding aromatic amines using polymer-supported hydrazine hydrate over iron oxide hydroxide catalyst. *Green Chemistry* **8**, 868-870, (2006).

14   Shi, Q., Lu, R., Lu, L., Fu, X. & Zhao, D. Efficient reduction of nitroarenes over nickel-iron mixed oxide catalyst prepared from a nickel-iron hydrotalcite precursor. *Advanced Synthesis & Catalysis* **349**, 1877-1881, (2007).

15   Wang, X. K. *et al.* Heterogeneous catalytic transfer partial-hydrogenation with formic acid as hydrogen source over the schiff-base modified gold nano-catalyst. *Catalysis Letters* **147**, 517-524, (2017).

16   Pogorelic, I. *et al.* Rapid, efficient and selective reduction of aromatic nitro compounds with sodium borohydride and Raney nickel. *J. Mol. Catal. A - Chem.* **274**, 202-207, (2007).

17   Rahman, A. & Jonnalagadda, S. B. Swift and selective reduction of nitroaromatics to aromatic amines with Ni–boride–silica catalysts system at low temperature. *Catalysis Letters* **123**, 264-268, (2008).

18   Corma, A. & Serna, P. Chemoselective hydrogenation of nitro compounds with supported gold catalysts. *Science* **313**, 332-334, (2006).

19   Wei, H. *et al.* FeO$_x$-supported platinum single-atom and pseudo-single-atom catalysts for chemoselective hydrogenation of functionalized nitroarenes. *Nature Communications* **5**, 5634 - 5642, (2014).

20   Wei, H. *et al.* Remarkable effect of alkalis on the chemoselective hydrogenation of functionalized nitroarenes over high-loading Pt/FeO$_x$ catalysts. *Chemical Science* **8**, 5126-5131, (2017).

21   Sankar, M. *et al.* Synthesis of stable ligand-free gold-palladium nanoparticles using a simple excess anion method. *ACS Nano* **6**, 6600-6613, (2012).

22   Zanella, R., Louis, C., Giorgio, S. & Touroude, R. Crotonaldehyde hydrogenation by gold supported on TiO$_2$: structure sensitivity and mechanism. *Journal of Catalysis* **223**, 328-339, (2004).

23   Cargnello, M. *et al.* Efficient removal of organic ligands from supported nanocrystals by fast thermal annealing enables catalytic studies on well-defined active phases. *Journal of the American Chemical Society* **137**, 6906-6911, (2015).

24   Freakley, S. J. *et al.* Palladium-tin catalysts for the direct synthesis of H$_2$O$_2$ with high selectivity. *Science* **351**, 965-968, (2016).

25   Chen, C., Cao, J. J., Cargnello, M., Fornasiero, P. & Gorte, R. J. High-temperature calcination improves the catalytic properties of alumina-supported Pd@ceria prepared by self assembly. *Journal of Catalysis* **306**, 109-115, (2013).

26   Matos, J. *et al.* In situ coarsening study of inverse micelle-prepared Pt nanoparticles supported on gamma-Al$_2$O$_3$: pre-treatment and environmental effects. *Physical Chemistry Chemical Physics* **14**, 11457-11467, (2012).

27   Kim, G. J., Kwon, D. W. & Hong, S. C. Effect of Pt particle size and valence state on the performance of Pt/TiO$_2$ catalysts for CO oxidation at room temperature. *Journal of Physical Chemistry C* **120**, 17996-18004, (2016).

28   Zimmermann, R. *et al.* Electronic structure of 3d-transition-metal oxides: On-site Coulomb repulsion versus covalency. *Journal of Physics-Condensed Matter* **11**, 1657-1682, (1999).

29   Riggs, W. M. X-ray photoelectron spectrometry of platinum compounds. *Analytical Chemistry* **44**, 830-832, (1972).

30   Moulder, J. F., Stickle, W. F., Sobol, P. E. & Bomben, K. D. *Handbook of X-ray Photoelectron Spectroscopy*. (Perkin-Elmer Corporation, 1992).

31   Naumkin, A. V., Kraut-Vass, A., Gaarenstroom, S. W. & Powell, C. J. (National Institute of Standards and Technology, Gaithersburg MD, 2000).

32   Janin, E. *et al.* Hydrogen adsorption on the Pt(111)(3×3) R30° Sn surface alloy studied by high resolution core level photoelectron spectroscopy. *Applied Surface Science* **99**, 371-378, (1996).

33   Brown, M., Peierls, R. E. & Stern, E. A. White lines in X-ray absorption. *Physical Review B* **15**, 738-744, (1977).

34   Koningsberger, D. & Prins, R. *X-ray absorption: Principles, applications, techniques of EXAFS, SEXAFS, and XANES.* (Wiley, 1988).

35   Penner-Hahn, J. E. X-ray absorption spectroscopy in coordination chemistry. *Coordination Chemistry Reviews* **190**, 1101-1123, (1999).

36   de Groot, F. High-resolution X-ray emission and X-ray absorption spectroscopy. *Chemical Reviews* **101**, 1779-1808, (2001).

37   Yoshida, H., Nonoyama, S., Yazawa, Y. & Hattori, T. Quantitative determination of platinum oxidation state by XANES analysis. *Physica Scripta* **T115**, 813-815, (2005).

38   Hyde, T. I. *et al.* X-ray absorption spectroscopic studies of platinum speciation in fresh and road aged light-duty diesel vehicle emission control catalysts. *Platinum Metals Review* **55**, 233-245, (2011).

39   Kim, M. Y., You, Y. S., Han, H. S. & Seo, G. Preparation of highly dispersed platinum catalysts impregnated on titania-incorporated silica support. *Catalysis Letters* **120**, 40-47, (2008).

40   Beale, A. M. & Weckhuysen, B. M. EXAFS as a tool to interrogate the size and shape of mono and bimetallic catalyst nanoparticles. *Physical Chemistry Chemical Physics* **12**, 5562-5574, (2010).

41   Raskó, J. CO-induced surface structural changes of Pt on oxide-supported Pt catalysts studied by DRIFTS. *Journal of Catalysis* **217**, 478-486, (2003).

42   Zafeiratos, S., Papakonstantinou, G., Jacksic, M. M. & Neophytides, S. G. The effect of Mo oxides and TiO_2 support on the chemisorption features of linearly adsorbed CO on Pt crystallites: an infrared and photoelectron spectroscopy study. *Journal of Catalysis* **232**, 127-136, (2005).

43   DeRita, L. *et al.* Catalyst architecture for stable single atom dispersion enables site-specific spectroscopic and reactivity measurements of CO adsorbed to Pt

atoms, oxidized Pt clusters, and metallic Pt clusters on TiO_2. *Journal of the American Chemical Society* **139**, 14150-14165, (2017).

44   Thang, H. V., Pacchioni, G., DeRita, L. & Christopher, P. Nature of stable single atom Pt catalysts dispersed on anatase TiO_2. *Journal of Catalysis* **367**, 104-114, (2018).

45   Stakheev, A. Y., Shpiro, E. S., Tkachenko, O. P., Jaeger, N. I. & Schulz-Ekloff, G. Evidence for monatomic platinum species in H-ZSM-5 from FTIR spectroscopy of chemisorbed CO. *Journal of Catalysis* **169**, 382-388, (1997).

46   S. J. Tauster, S. C. F., and R. L. Garten. Strong metal-support interactions. Group 8 noble metals supported on TiO_2. *Journal of the American Chemical Society* **100**, 170-175, (1978).

47   Vannice, M. A. & Sen, B. Metal support effects on the intramolecular selectivity of crotonaldehyde hydrogenation over platinum. *Journal of Catalysis* **115**, 65-78, (1989).

48   Baker, L. R. *et al.* Furfuraldehyde hydrogenation on titanium oxide-supported platinum nanoparticles studied by sum frequency generation vibrational Ssectroscopy: Acid–base catalysis explains the molecular origin of strong metal–support interactions. *Journal of the American Chemical Society* **134**, 14208-14216, (2012).

49   Boronat, M. & Corma, A. Origin of the different activity and selectivity toward hydrogenation of single metal Au and Pt on TiO_2 and bimetallic Au-Pt/TiO_2 catalysts. *Langmuir* **26**, 16607-16614, (2010).